2

MICROSTRIP ANTENNA – A GENERALIZED TRANSMISSION LINE

A. K. Bhattacharyya, L. Shafai, and R. Garg

2.1 Introduction

Microstrip antennas represent the latest development in the pursuit of low cost, very thin flat antenna structures. These antennas consist of metallic patches printed onto a substrate backed by a conducting ground plane. This definition of a microstrip antenna may admit a wide range of the thickness and the dielectric constant of the substrate.

Microstrip antennas have several advantages compared to the conventional microwave antennas. Some of the principal advantages are: light weight with planar configurations and low fabrication cost. Due to the low volume of microstrip antennas, they can be mounted onto aero-space vehicles making them flush with the vehicle surface. They may also be used as the feeds of reflector antennas or as the elements in an array. Some disadvantages are: limited band width and low power handling capability.

There are several analytical techniques available in the literature [1-3] for the analyses of microstrip antennas. Among them the transmission line model [1] is the simplest. This model was proposed by Munson [4] and Derneryd [5,6] separately to analyze a rectangular patch antenna fed at the center of a radiating wall. In this model, the rectangular patch is considered to be a section of a uniform microstrip transmission line loaded with impedances at the two ends. These impedances represent the radiated power that emanates from the open ends and the stored energy in the fringing fields. These impedances are normally calculated by considering a radiating wall to be equivalent to a narrow rectangular grounded slot. The length of the slot is assumed to be equal to the width of the patch and the width of the slot is taken as the thickness of the substrate [6]. The conventional transmission line theory is then employed to determine the input impedance of the antenna. The radiation patterns of the patch are assumed to be the same as that of an array of two narrow slots separated by a distance equal to the length of the patch [1,2,6].

The above transmission line model is very simple conceptually. However, the model has a few limitations. These are:

(i) the model is applicable for rectangular patches only

(ii) mutual coupling between the radiating edges is ignored

(iii) effects of substrate on radiation are not considered

The effect of dielectric substrate can be incorporated in the model if the radiating slots are considered to be located inside the dielectric layer of a grounded dielectric substrate [7] instead of considering them lying on a ground plane. Also, the mutual coupling between the two edges can be incorporated to a certain extent by taking the active conductance (instead of self wall conductance) of the radiating walls as done in [6]. In order to determine the active conductance, the ratio of the aperture fields should be known. In [6], the ratio is assumed to be equal to unity. This assumption is valid for a rectangular patch etched

on a very thin substrate, when operating at the resonant frequency. Away from the resonance and with a thicker substrate the ratio will be different from unity and the model will yield inaccurate results.

In [20] Pues and Van de Capelle improved the transmission line model of a rectangular patch by incorporating the mutual coupling effect into the equivalent circuit of the patch. They introduced two voltage dependent current generators at the two ends of the patch which take care of the coupling. Numerical results show good agreement with the experiment.

The limitations of the conventional transmission line model are overcome in a newly proposed model [8] known as the Generalized Transmission Line Model (GTLM). Contrary to the conventional transmission line model (CTLM), the GTLM can be applied to a host of microstrip patch antennas normally used in practice [8]. In addition, this new model considers the mutual coupling aspect between the radiating apertures systematically in its exact form without any approximation or assumption. Moreover, the effect of dielectric substrate can be incorporated easily in the GTLM.

In this chapter the theoretical background of the generalized transmission line model is reviewed. Analyses of various microstrip antennas using the GTLM are considered briefly. Finally, theoretical and experimental results of some useful microstrip antenna structures are presented.

2.2 The Generalized Transmission Line Model

The generalized transmission line model (GTLM) consists of a section of transmission line representing the lossless patch. The power radiated through the radiating apertures (walls) is taken into consideration by means of radiation impedances terminating at the two ends of the transmission line. The mutual coupling effect between the radiating apertures is taken care of by means of an additional impedance joining the two ends of the transmission line. The transmission line together with the above impedances yields the equivalent circuit of the structure from which all informations regarding the radiation characteristics are obtained. The GTLM, in principle, can be applied to the microstrip patches which have seperable geometries. The majority number of the practically used patches comes under this category. The theoretical background of the model is considered in the following subsection.

a. Theoretical Background of the GTLM

Two different types of possible microstrip patch configurations with separable geometries are shown in Fig. 2.1. The patch in Fig. 2.1(a) has two radiating edges defined by $u = u_1$ and $u = u_2$ in terms of the curvilinear coordinate $(u - v)$ system. On the other hand, the patch in Fig. 2.1(b) has four edges given by $u = u_1$, $u = u_2$, $v = v_1$ and $v = v_2$, respectively. The annular ring is an example of the first kind (Fig. 2.1(a)) and a rectangular patch is an example of the second kind. The circular patch has only one radiating edge and comes under the first kind when the inner radiating contour $(u = u_1)$ has vanishingly small area (converges to a point).

In order to develop the model, we start with the field configurations under the patch metallization. The longitudinal component (z-component) of the electric field underneath the patch is a solution of the following wave equation (a time dependence $e^{j\omega t}$ is assumed):

$$\nabla^2 E_z + k_1^2 E_z = 0 \tag{1}$$

where ∇^2 represents the Laplacian operator and k_1 is the wave number inside the substrate on which the patch is etched. In a practical microstrip antenna, the thickness, h, of the dielectric substrate is very small compared to the wavelength, λ_ϵ, in the dielectric medium (typically $h \leq \lambda_\epsilon/50$). The z-directed electric field, E_z, therefore can be regarded as a constant along z. Equation (1) then can be written in the curvilinear coordinate system as [9]

$$\frac{1}{h_1 h_2}\left[\frac{\partial}{\partial u}\left(\frac{h_2}{h_1}\frac{\partial E_z}{\partial u}\right) + \frac{\partial}{\partial v}\left(\frac{h_1}{h_2}\frac{\partial E_z}{\partial v}\right)\right] + k_1^2 E_z = 0 \tag{2}$$

where h_1 and h_2 are the scale factors along u and $v-$directions, respectively and are

$$h_1 = \left|\frac{\partial \bar{r}}{\partial u}\right|, \quad h_2 \left|\frac{\partial \bar{r}}{\partial v}\right|,$$

$\bar{r}$ being the position vector. It is assumed that the patch configurations under consideration are separable, i.e. the solution for E_z in (2) can be expressed as

$$E_z(u, v) = f_1(u)\, f_2(v). \tag{3}$$

Substituting (3) in (2) and dividing the equation by $f_1(u)\, f_2(v)$, one obtains

$$\frac{1}{h_1 h_2}\left[\frac{1}{f_1}\frac{\partial}{\partial u}\left(\frac{h_2}{h_1}\frac{\partial f_1}{\partial u}\right) + \frac{1}{f_2}\frac{\partial}{\partial v}\left(\frac{h_1}{h_2}\frac{\partial f_2}{\partial v}\right)\right] + k_1^2 = 0 \tag{4}$$

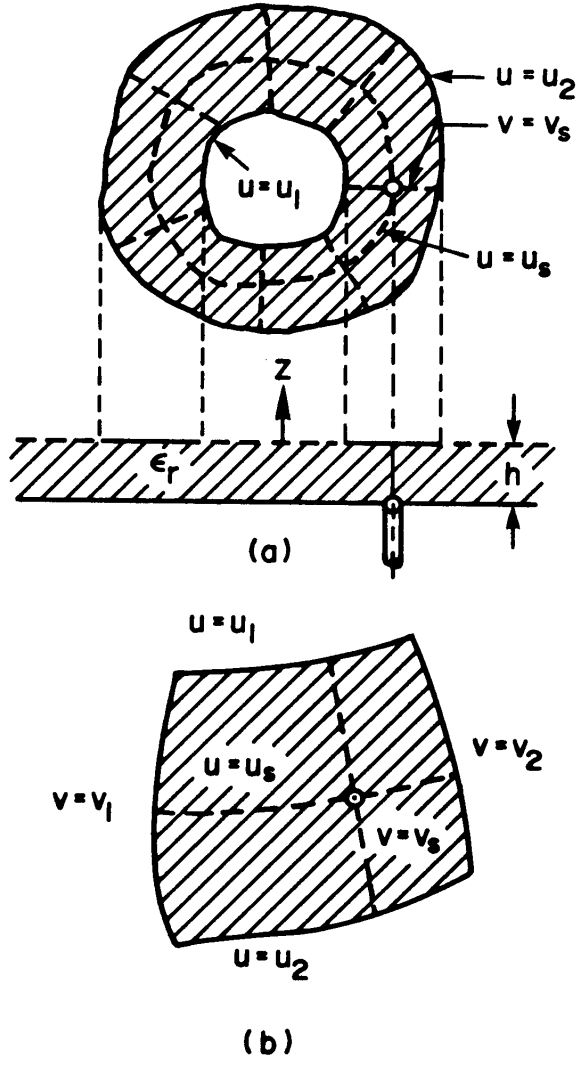

Figure 2.1 General configurations of microstrip patches with separable geometry. (a) Two edges (b) Four edges.

Let $h_2/h_1 = p(u,v)$ and $h_1 h_2 = q(u,v)$. Then equation (4) becomes

$$\frac{p}{f_1}\frac{\partial^2 f_1}{\partial u^2} + \frac{1}{f_1}\frac{\partial p}{\partial u}\frac{\partial f_1}{\partial u} + \frac{1}{f_2 p}\frac{\partial^2 f_2}{\partial v^2} - \frac{1}{f_2}\left(\frac{1}{p^2}\frac{\partial p}{\partial v}\right)\frac{\partial f_2}{\partial v} + k_1^2 q = 0 \quad (5)$$

The above bivariate equation can be separated out into two single variable differential equations if either

$$\text{(i)} \quad p(u,v) = g(u)\, f(v)$$
$$\text{and } p(u,v)\, q(u,v) = [m_1(u) + m_2(v)]\, f^2(v) \qquad (6a)$$

$$\text{or (ii)} \quad p(u,v) = g(u)/f(v)$$
$$\text{and } q(u,v)/p(u,v) = [m_1(u) + m_2(v)]/g^2(u) \qquad (6b)$$

Apparently (6a) and (6b) appear to be two distinct criteria for the separability of (5). However, if one solves for h_1 and h_2 either from (6a) or from (6b), one can see that they assume similar forms. Therefore, without the loss of generality, one can consider that (6a) holds. Equation (5) can then be separated as

$$\frac{g^2}{f_1}\frac{\partial^2 f_1}{\partial u^2} + \frac{g}{f_1}\frac{\partial g}{\partial u}\frac{\partial f_1}{\partial u} + k_1^2 m_1(u) = \alpha^2 \qquad (7a)$$

and

$$\frac{1}{f^2}\frac{1}{f_2}\frac{\partial^2 f_2}{\partial v^2} - \frac{1}{f^3}\frac{1}{f_2}\frac{\partial f}{\partial v}\frac{\partial f_2}{\partial v} + k_1^2 m_2(v) = -\alpha^2 \qquad (7b)$$

where α is a constant, independent of u and v. Equations (7a) and (7b) can be rewritten as

$$\frac{\partial^2 f_1}{\partial u^2} + \frac{1}{g}\frac{\partial g}{\partial u}\frac{\partial f_1}{\partial u} + \left(\frac{k_1^2 m_1 - \alpha^2}{g^2}\right) f_1 = 0 \qquad (8)$$

and

$$\frac{\partial^2 f_2}{\partial v^2} - \frac{1}{f}\frac{\partial f}{\partial v}\frac{\partial f_2}{\partial v} + \left(k_1^2 m_2 + \alpha^2\right) f^2 f_2 = 0 \qquad (9)$$

Equations (8) and (9) are second order non linear (in general) differential equations. Each of them will have two independent solutions. Let $x_1(u)$ and $x_2(u)$ be two solutions of (8). The general solution for E_z will be then

$$E_z(u,v) = \left\{ \begin{matrix} x_1(u) \\ x_2(u) \end{matrix} \right\} f_2(v) \qquad (10)$$

With E_z determined as above, the magnetic field components inside the structure is obtained through the Maxwell equation $\nabla \times \overline{E} = -j\omega\mu\overline{H}$. The magnetic field components are given by

$$-j\omega\mu H_u = \frac{1}{h_2}\frac{\partial E_z}{\partial v} = \frac{1}{h_2} f_1(u) f_2'(v) \tag{11}$$

$$-j\omega\mu H_v = -\frac{1}{h_1}\frac{\partial E_z}{\partial u} = -\frac{1}{h_1} f_1'(u) f_2(v) \tag{12}$$

where a prime indicates the derivative of the function with respect to the argument.

b. Transmission Line Equations

It has been stated earlier that a patch can be made equivalent to a transmission line section. The transmission line voltage and the transmission line current will be defined here.

In accordance to the GTLM, the transmission line is taken along the line joining two radiating apertures. The direction of the transmission line in the case of a patch with two edges (Fig. 2.1(a)) is unique (along u-direction). However, for the patch configuration shown in Fig. 2.1(b) there may be two possible directions of the transmission line; along the v = constant contour (joining two apertures at $u = u_1$ and $u = u_2$) and along u = constant contour (joining two apertures at $v = v_1$ and $v = v_2$). In principle, one can select any one of the above two directions. The effect of radiation of two connecting apertures will appear in the equivalent circuit through terminating loads. The effect of the other two apertures can be incorporated by considering the transmission line to be leaky. However, in order to simplify the analysis, one should consider the transmission line joining the two apertures which radiate major portion of the power. It is not difficult to make out which of the apertures are radiating less power, because it can be easily ascertained from the aperture field distribution (see example in Section 1.6a).

b.1. Transmission line in u-direction

In order to characterize a transmission line, the transmission line voltage and the transmission line current should be defined. The definitions of these quantitites should be such that they follow the transmission line equation pair (telegraphic equations). For a transmission

line in the u-direction, the line voltage is defined as

$$V = E_z(u, v) = f_1(u)\, f_2(v) \tag{13}$$

and the line current is defined as

$$I = -h_2 H_v \text{ (along the positive } u - \text{direction)}. \tag{14}$$

Substituting in (12), one has

$$I = -\frac{h_2}{j\omega\mu h_1} \cdot f_1'(u)\, f_2(v). \tag{15}$$

Differentiating (13) with respect to u, one gets

$$\frac{\partial V}{\partial u} = f_1'(u)\, f_2(v) = -j\omega\mu \frac{h_1}{h_2} I$$

or

$$\frac{\partial V}{\partial u} = -\frac{j\omega\mu}{p} I = -\frac{j\omega\mu}{g(u)\, f(v)} \tag{16}$$

Combining (8) and (13), we can have

$$\frac{\partial^2 V}{\partial u^2} + \frac{1}{g}\frac{\partial g}{\partial u}\frac{\partial V}{\partial u} + \frac{(k_1^2 m_1 - \alpha^2)}{g^2} V = 0$$

or

$$\frac{\partial}{\partial u}\left(g \frac{\partial V}{\partial u}\right) + \frac{(k_1^2 m_1 - \alpha^2)}{g} V = 0 \tag{17}$$

Substituting the expression of $\dfrac{\partial V}{\partial u}$ from (16) to (17) one has

$$\frac{\partial I}{\partial u} - \frac{f(v)(k_1^2 m_1 - \alpha^2)}{j\omega\mu g(u)} V = 0 \tag{18}$$

Equations (16) and (18) are the transmission line equations. The transmission line parameters are:

$$\text{shunt admittance/length} \equiv -\frac{\left[k_1^2 m_1(u) - \alpha^2\right] f(v)}{j\omega\mu g(u)} \tag{19}$$

$$\text{series impedance/length} \equiv \frac{j\omega\mu}{g(u) f(v)} \tag{20}$$

The parameters being functions of u, the equivalent circuit of the patch is a non-uniform transmission line. Expressions of $f(v), g(u)$ and $m_1(u)$ are dictated by the geometry of the separable patch. The constant α, however, depends on the 'mode' of operation. The value of α is obtained from the solution of (9) with appropriate boundary conditions. When the radiating contours are closed as in Fig. 2.1(a), the function $f_2(v)$ must be a periodic function of v and the values of α are discrete in nature. Each α is associated with a mode. Therefore, a transmission line mode is designated by a single index (corresponding to the value of α). When the radiating contours are not closed (as in Fig. 2.1(b)), the value of α, in general, will be complex due to leakage of power through the apertures at $v = v_1$ and $v = v_2$. Determination of the complex α will be considered later in an example. The line voltage and the line current of a transmission line in the v-direction will be considered next.

b.2. Transmission line in v-direction

For the transmission line in the v-direction, the line voltage is defined as $V = E_z$ and the line current is defined as

$$I = -\frac{h_2 H_u}{f(v)} \text{ (along the positive } v - \text{ direction)} \tag{21}$$

Combining (9), (11) and (21), we have

$$\frac{\partial V}{\partial v} = j\omega\mu\, f(v) I \tag{22}$$

and

$$\frac{\partial I}{\partial v} = -\frac{f(v)}{j\omega\mu}\left(k_1^2 m_2(v) + \alpha^2\right) V \tag{23}$$

Therefore, the definitions of the line voltage and the line current follow the transmission line equations in the v-direction. The line parameters of the non-uniform transmission line can be obtained from (22) and (23).

In the preceeding sections, the line voltages and the line currents of two possible transmission lines are defined. The equivalent circuit of a non-uniform transmission line section will be obtained in the section that follows.

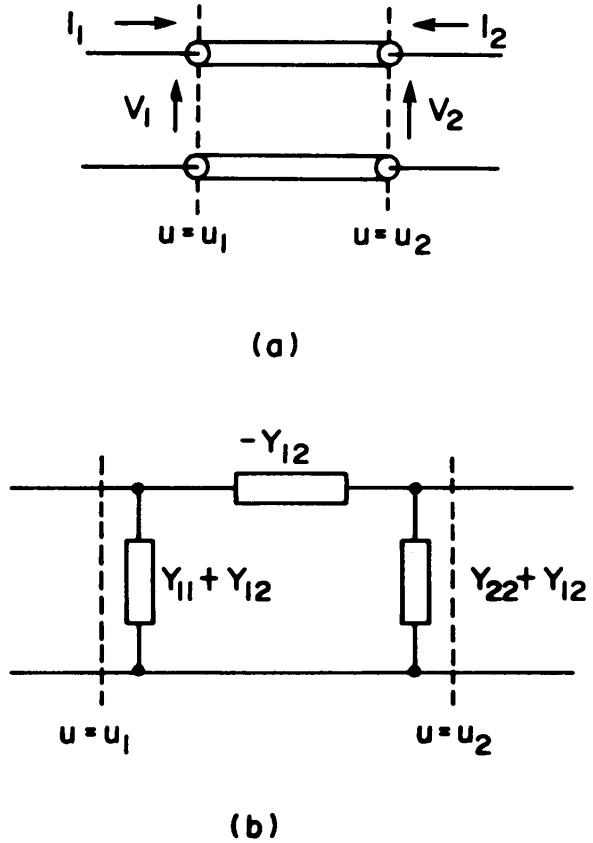

Figure 2.2 (a) A non uniform transmission line section. (b) Equivalent Π-network of the section.

c. Equivalent Circuit of a Non-uniform Transmission Line Section

In this section, the equivalent Π-network of a transmission line section will be obtained. We shall concentrate on the u-directed transmission line here. The equivalent Π-network of a transmission line in the v-direction can be obtained in a similar manner.

A transmission line section confined in the region $u_1 < u < u_2$ (non uniform, in general) and its equivalent Π-network are shown in Fig. 2.2. Elements of the equivalent Π-network are obtained from the

Y-matrix of the transmission line. The Y-matrix is defined by

$$\begin{bmatrix} I_1 \\ I_2 \end{bmatrix} = \begin{bmatrix} Y_{11} & Y_{12} \\ Y_{21} & Y_{22} \end{bmatrix} \begin{bmatrix} V_1 \\ V_2 \end{bmatrix} \tag{24}$$

where I_1, I_2 are the port currents at the two ports of the transmission line. Directions of these currents are shown in Fig. 2.2. V_1, V_2 are the port voltages. The elements of the Y-matrix are obtained from the following equations:

$$\begin{aligned} Y_{11} &= I_1/V_1 \text{ (when } V_2 = 0) \\ Y_{12} &= I_1/V_2 \text{ (when } V_1 = 0) \\ Y_{21} &= I_2/V_1 \text{ (when } V_2 = 0) \\ Y_{22} &= I_2/V_2 \text{ (when } V_1 = 0) \end{aligned}$$

Here, V is the line voltage and is given by

$$V = E_z = \Big\{ A x_1(u) + B x_2(u) \Big\} f_2(v) \tag{25}$$

and the line current along u is given by

$$I = -\frac{1}{j\omega\mu} \frac{h_2}{h_1} \Big\{ A x_1'(u) + B x_2'(u) \Big\} f_2(v) \tag{26}$$

where A and B are two constants, and $x_1(u)$ and $x_2(u)$ are two independent solutions of (8). Now, $V_2 = V(u = u_2) = 0$ demands that

$$B/A = -x_1(u_2)/x_2(u_2)$$

The expression for Y_{11} thus becomes

$$Y_{11} = \frac{I_1}{V_1} = \frac{I(u = u_1)}{V(u = u_1)} = -\frac{h_2}{j\omega\mu h_1} \left\{ \frac{x_2(u_2)x_1'(u_1) - x_1(u_2)x_2'(u_1)}{x_2(u_2)x_1(u_1) - x_1(u_2)x_2(u_1)} \right\} \tag{27}$$

Similarly,

$$\begin{aligned} Y_{22} &= -\frac{I(u = u_2)}{V(u = u_2)} \qquad (\text{when } V(u = u_1) = 0) \\ &= \frac{1}{j\omega\mu} \frac{h_2}{h_1} \left\{ \frac{x_2(u_1)x_1'(u_2) - x_1(u_1)x_2'(u_2)}{x_2(u_1)x_1(u_2) - x_1(u_1)x_2(u_2)} \right\} \end{aligned} \tag{28}$$

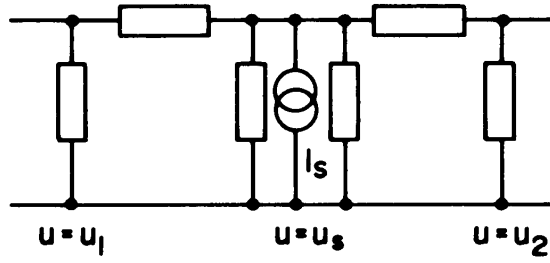

Figure 2.3 Equivalent circuit representing the patch.

Note that the value of h_2/h_1 in (27) should be evaluated at $u = u_1$ in the case of (27) whereas the above quantity should be evaluated at $u = u_2$ in the case of (28).

The expression for Y_{12} is given by

$$Y_{12} = \frac{I(u = u_1)}{V(u = u_2)} \qquad (\text{when } V(u = u_1) = 0)$$

Now, $V(u = u_1) = 0$ yields $B/A = -x_1(u_1)/x_2(u_1)$. The final expression for Y_{12} then becomes

$$\begin{aligned} Y_{12} &= -\frac{1}{j\omega\mu}\frac{h_2}{h_1}\left\{\frac{x_1'(u_1)x_2(u_1) - x_1(u_1)x_2'(u_1)}{x_2(u_1)x_1(u_2) - x_2(u_2)x_1(u_1)}\right\} \\ &= -\frac{1}{j\omega\mu}\frac{h_2}{h_1}\frac{W(u_1)}{\{x_2(u_1)x_1(u_2) - x_2(u_2)x_1(u_1)\}} \end{aligned}$$

where $W(u)$ is the 'Wronskian' of (8). In Appendix A, the Wronskian is determined and is found to be equal to $W(u) = C/g(u)$, where C is a constant which depends on the choice of $x_1(u)$ and $x_2(u)$. The expression for Y_{12} thus reduces to

$$Y_{12} = -\frac{C}{j\omega\mu f(v)}\{x_2(u_1)x_1(u_2) - x_2(u_2)x_1(u_1)\}^{-1} \qquad (29)$$

In a similar way, one can derive the expression for Y_{21} and can verify that

$$Y_{12} = Y_{21} \qquad (30)$$

The above relation confirms the transmission line section to be a 'reciprocal' device and therefore a Π-network model of the device is possible. This relation also justifies the definition of the line voltage and line currents used in equations (13) and (14), respectively. When a patch is excited by a source placed at $u = u_s$, the patch is equivalent to two transmission line sections confined in the regions defined as $u_1 < u < u_s$ and $u_s < u < u_2$, respectively. Each of the transmission line section will have a Π-network as shown in Fig. 2.2. The elements of Y-matrix for the section confined in the region $u_1 < u < u_s$ can be obtained by replacing u_2 by u_s in (27), (28) and (29). Similarly, for the section in the region $u_s < u < u_2$, the matrix elements will be obtained after replacing u_1 by u_s in these equations. The equivalent circuit of the patch with the source is shown in Fig. 2.3.

In this section, the equivalent network of the patch is developed. This network takes care of the power stored under the patch metallization and the dielectric loss for an imperfect dielectric substrate and the loss of power due to the leakage through the side walls at $v = v_1$, and $v = v_2$. In order to incorporate the radiated power through the main radiating apertures, the circuit should be terminated with appropriate radiation impedances. This will be considered next.

d. Effects of Radiation

The effect of radiation through the two main radiating apertures (at $u = u_1$ and at $u = u_2$) can be incorporated into the equivalent circuit of Fig. 2.3. A radiating aperture may be characterized by an equivalent admittance, the susceptance being due to the stored energy in the fringing fields and the conductance is due to the radiation loss. In order to determine the wall admittance the magnetic current model may be used. In the magnetic current model, an aperture is replaced by its equivalent magnetic current. The electromagnetic fields radiated by the equivalent magnetic current are the same as that of the aperture. Since we have two apertures, in general, there should be two equivalent magnetic current sources. The active wall admittance on the wall at $u = u_1$ will be

$$y_1^a = -\frac{I_t(u_1)}{V(u_1)} \tag{31}$$

where $I_t(u_1)$ is the total induced line currents on the aperture at $u = u_1$ due to the magnetic current sources at $u = u_1$ and $u = u_2$, respectively.

According to the definition of the line current in (14), we have

$$I_t(u_1) = -h_2 H_{vt}(u_1)$$

where $H_{vt}(u_1)$ is the total induced magnetic fields along v on the aperture at $u = u_1$. This field is a summation of the self magnetic field, $H_{vs}(u_1)$, which is generated by the source at $u = u_1$ and the coupled field, $H_{vm}(u_1, u_2)$, which is generated by the source at $u = u_2$ on the aperture at $u = u_1$. Therefore,

$$H_{vt}(u_1) = H_{vs}(u_1) + H_{vm}(u_1, u_2) \tag{32}$$

The active wall admittance thus becomes

$$y_1^a = \frac{h_2 H_{vs}(u_1)}{E_z(u_1)} + \frac{h_2 H_{vm}(u_1, u_2)}{E_z(u_1)} \tag{33}$$

Let us define the self admittance of the radiating wall at $u = u_1$ as

$$y_1^s = \frac{h_2 H_{vs}(u_1)}{E_z(u_1)} \tag{34}$$

and the mutual admittance between the two walls as

$$y_{21}^m = -\frac{h_2 H_{vm}(u_1, u_2)}{E_z(u_1)} \tag{35}$$

The negative sign in (35) is taken since the equivalent magnetic currents at $u = u_1$ and at $u = u_2$ are oppositely directed. In addition, from the expression of the mutual admittance, defined in (34), one can obtain the self admittance as a special case, when u_2 approaches u_1. Using (34) and (35) in (33), one has

$$y_1^a = y_1^s - y_{21}^m \frac{E_z(u_2)}{E_z(u_1)} = y_1^s - y_{21}^m \frac{V_2}{V_1} \tag{36}$$

where V_2 and V_1 are the line voltages at port 2 and port 1, respectively. Rearranging (36), one has

$$y_1^a = (y_1^s - y_{21}^m) + \frac{V_1 - V_2}{V_1} y_{21}^m \tag{37}$$

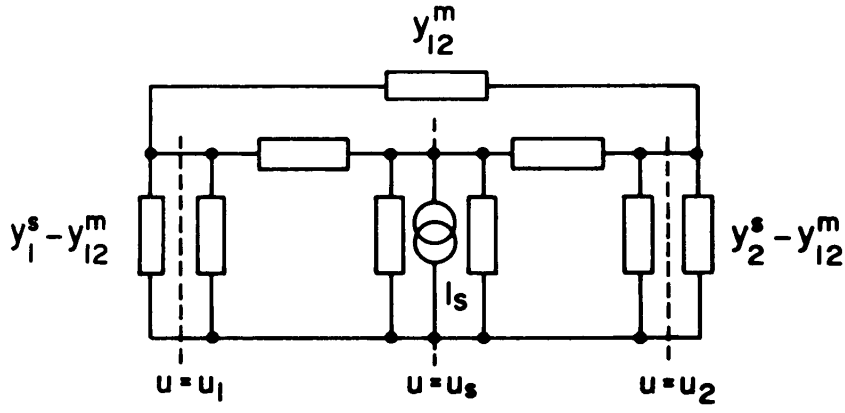

Figure 2.4 Complete equivalent circuit of the patch antenna for a given transmission line mode.

Similarly for the port 2 (at $u = u_2$), we will have

$$y_2^a = (y_2^s - y_{12}^m) + \frac{V_2 - V_1}{V_2} y_{12}^m \tag{38}$$

The 'reciprocity' demands that $y_{12}^m = y_{21}^m$. Therefore, (37) and (38) lead to an equivalent circuit shown in Fig. 2.4. This circuit can be used to determine the input impedance seen by the source I_s and aperture voltages (voltages at $u = u_1$ and $u = u_2$) from which the radiation characteristics of a patch can be determined. Note that the equivalent circuit in Fig. 2.4 represents a single mode (for a given value of α in (8)). Each mode will have a circuit shown in Fig. 2.4. The source current I_s is related to the feed current, and the mode of operation. The input impedance seen by the feed is proportional to the impedance seen by I_s, for a given mode of operation.

In order to determine the input impedance seen by the source I_s, the circuit in Fig. 2.4 can be simplified using the star-delta and delta-star transformations as necessary. The impedance seen by the feed current will be obtained if the relation between I_s and the feed current is known. This relation will be established in the following subsection. Expression for the input impedance will also be considered.

2.3 Input Impedance

Figure 2.4 yields the impedance of a single mode seen by the source current I_s. The impedance seen by the feed current will be obtained once the relation between I_s (called the source current for a given mode) and the feed current is known.

Suppose $\hat{z}I_0(v)$ is the feed current distribution (assumed to be a surface current lying on the ficticious surface defined as $u = u_s$ where $I_0(v)$ is a function of v only). The magnetic field will be discontinuous at $u = u_s$ due to the presence of the feed current. For a given mode, let the magnetic fields at $u = u_s^+$ and at $u = u_s^-$ be

$$H_v^{(\alpha)}(u_s^+) = A_\alpha^+ f_2^\alpha(v) \tag{39}$$

$$H_v^{(\alpha)}(u_s^-) = A_\alpha^- f_2^\alpha(v) \tag{40}$$

where $f_2^{(\alpha)}(v)$ is a solution of (9) for a given α. The discontinuity of the magnetic fields yields

$$\sum_\alpha \left[H_v^\alpha(u_s^+) - H_v^\alpha(u_s^-)\right] = I_0(v) \tag{41}$$

Now $-h_2 H_v^{(\alpha)}(u_s^+)$ is the line current supplied by the source to the region $u > u_s$ and $h_2 H_v^{(\alpha)}(u_s^-)$ is the line current supplied by the source to the region $u < u_s$. Therefore,

$$\begin{aligned} I_s &= -h_2 H_v^{(\alpha)}(u_s^+) + h_2 H_v^{(\alpha)}(u_s^-) \\ &= -h_2 \left[A_\alpha^+ - A_\alpha^-\right] f_2^{(\alpha)}(v) = -h_2 B_\alpha f_2^{(\alpha)}(v) \quad \text{(say)} \end{aligned} \tag{42}$$

Now the total current supplied for various α should be equal to the feed current $I_0(v)$. Therefore,

$$-\sum_\alpha B_\alpha f_2^{(\alpha)}(v) = I_0(v) \tag{43}$$

It has been shown in Appendix B that the set of functions $f_2^{(\alpha)}(v)$ for various α form an orthogonal set and

$$\int_{v_1}^{v_2} f(v) f_2^{(\alpha)}(v) f_2^{(\alpha')}(v)\, dv = 0 \text{ when } \alpha \neq \alpha' \tag{44}$$

Using this orthogonality property, one can have

$$-B_\alpha \int_{v_1}^{v_2} f(v) \left[f_2^{(\alpha)}(v)\right]^2 dv = \int_{v_1}^{v_2} f(v)\, f_2^{(\alpha)}(v) I_0(v) dv$$

or

$$B_\alpha = -\frac{\displaystyle\int_{v_1}^{v_2} f(v)\, f_2^{(\alpha)}(v)\, I_0\, dv}{\displaystyle\int_{v_1}^{v_2} f(v) \left[f_2^{(\alpha)}(v)\right]^2 dv} \tag{45}$$

Substituting B_α in (42), we get the relation between the source current I_s and the feed current $I_0(v)$. In particular, when the patch is excited by a probe, the function $I_0(v)$ may be approximated as

$$I_0(v) = I_0 \delta(v - v_s)/h_2(v)$$

where (u_s, v_s) is the feed location. In that situation, the value of B_α will be

$$B_\alpha = -\frac{I_0 \frac{f(v_s)}{h_2}\, f_2^{(\alpha)}(v_s)}{\displaystyle\int_{v_1}^{v_2} f(v) \left[f_2^{(\alpha)}(v)\right]^2 dv}$$

and

$$I_s = \frac{f_2^{(\alpha)}(v) I_0\, f(v_s)\, f_2^{(\alpha)}(v_s)}{\displaystyle\int_{v_1}^{v_2} f(v) \left[f_2^{(\alpha)}(v)\right]^2 dv} \tag{46}$$

The input impedance seen by the feed is then

$$Z_{in} = -\frac{h\, E_z(u_s, v)}{I_0} = \frac{E_z}{I_s}\left(-\frac{hI_s}{I_0}\right) = -\frac{h\, I_s}{I_0} Z_s \tag{47}$$

where Z_s is the impedance seen by I_s in Fig. 2.4. The expression for I_s/I_0 can be substituted from (46) to (47) to obtain the impedance seen by the feed current I_0.

Equation (47) yields the input impedance seen by the feed current I_0 when only one transmission line mode is present. In order to obtain the total input impedance, individual impedances for all possible modes should be added together. However, if the resonant frequencies are not very close to each other as compared to the bandwidth

of the operating mode, the contribution of the off-resonant modes will be negligible near the resonance of the operating mode. On the other hand if some other modes are very close to the operating mode, those mode-impedances are to be added. A typical example of this kind is considered in section 2.6.b.

In order to determine the impedance seen by I_s in the equivalent circuit shown in Fig. 2.4, the self and mutual admittances are to be known. General expressions for these admittances will be obtained in the following section.

2.4 Self and Mutual Wall Admittances

In section 2.2.d, it has been mentioned that the magnetic current model can be used to determine the wall admittances of a patch antenna. In the magnetic current model [1], a patch is replaced by the equivalent magnetic current source at its periphery. The wall admittances of the patch is equivalent to the radiation admittances of the magnetic currents.

The mutual admittance between two edges is defined as

$$y_{12}^{m} = -\frac{h_2\, H_{vm}(u_1, u_2)}{E_z(u_2)} = \frac{h_2\, H_{vm}(u_2, u_1)}{E_z(u_1)} \tag{48}$$

where $E_z(u_1)\, f_2(v)$ and $E_z(u_2)\, f_2(v)$ are the aperture electric fields at $u = u_1$ and $u = u_2$, respectively. $H_{vm}(u_1, u_2)\, f_2(v)$ is the magnetic field at $u = u_1$ produced by the equivalent source at $u = u_2$.

The v-directed magnetic field H_{vm} at $u = u_1$ generated by the magnetic current source at $u = u_2$ can be determined using the Green's function technique. The expression for the magnetic field will be

$$\overline{H}_m(u_2, u_1) = \iint_{s_1} \overline{M}_1 \cdot \overline{\overline{G}}(r_2/r_1)\, ds_1$$

where $\overline{M}_1$ is the equivalent magnetic current on the aperture located at $u = u_1$ and is equal to $E_z(u_1)(\hat{z} \times \hat{u}_1)$. $\overline{\overline{G}}$ is the dyadic Green's function which relates the magnetic current to the magnetic field and s_1 is the surface area of the aperture at $u = u_1$. One can use the free space Green's function in (48) to determine the mutual admittance. However, in order to include the effect of dielectric substrate, Green's

function of a stratified media should be used. For a thin substrate and with low dielectric constant ($h\sqrt{\varepsilon_r}/\lambda o < .04$), the effect is negligibly small and the free space Green's function yields a good approximation to the mutual admittance.

In order to compute the mutual admittance one can use (48). However, to obtain an accurate result for the mutual admittance, one should use the stationary expression. Equation (48) does not yield a stationary expression for y_{12}^m. The stationary expression for the mutual admittance will be

$$y_{12}^m = \frac{\langle u_1, u_2 \rangle}{h\, P\, E_z(u_1)\, E_z(u_2)} \tag{49}$$

with

$$P = \int_{v_1}^{v_2} \Big[f_2(v) \Big]^2 \, dv$$

In (49) h is the substrate thickness and $\langle u_1, u_2 \rangle$ is the mutual reaction between the two magnetic current sources placed at $u = u_1$ and $u = u_2$, respectively. In Appendix C the stationary character of the above expression in (49) has been proved. In addition, since $\langle u_1, u_2 \rangle = \langle u_2, u_1 \rangle$, $y_{12}^m = y_{21}^m$. Equation (49) gives the mutual admittance when the radiating apertures are located at $u = u_1$ and $u = u_2$ curves. If the radiating apertures are in the location $v = v_1$ and $v = v_2$, the stationary expression for the mutual admittance becomes

$$y_{12}^m = \frac{\langle v_1, v_2 \rangle}{h\, E_z(v_1)\, E_z(v_2) \displaystyle\int_{u_1}^{u_2} \frac{f_1^2(u)}{g(u)}\, du} \tag{50}$$

where $E_z(v_1) f_1(u)$ and $E_z(v_2) f_1(u)$ are the electric fields at $v = v_1$ and $v = v_2$, respectively. Equation (49) should be used when the transmission line is along the u-direction and (50) should be used when the transmission line is along the v-direction. For the self admittances, one should use the self reaction instead of the mutual reaction in the numerators of (49) and (50).

2.5 Radiation Patterns

The radiation patterns of a patch can be determined once the aperture fields are known. The aperture fields are obtained from the

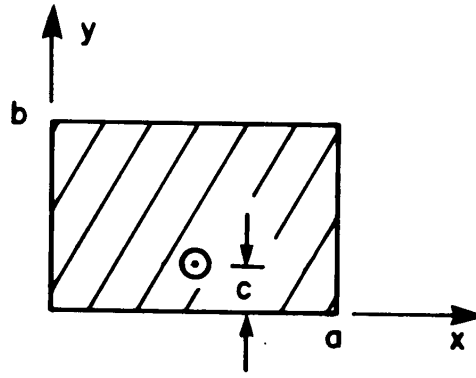

Figure 2.5 Geometry of a rectangular patch antenna.

equivalent circuit of the patch. The principle of equivalence is then employed to obtain the equivalent magnetic currents on the apertures. Using the Green's function technique one can derive the expression for the far radiated fields. For a thin dielectric substrate, the effect of dielectric on the radiated field will be negligibly small and one can use the free space Green's function in order to determine the far fields. However, when the substrate thickness is large ($h > \lambda/20$) the effects of the dielectric on the radiation pattern is substantial. In such cases, the Green function in the stratified media should be used. It is shown by Kong [10] that the effect of the dielectric substrate on the radiated field can be taken into account by multiplying a factor to the result obtained if the effect of the substrate is ignored.

So far, we have presented the theory of the generalized transmission line model. The application of the model for linearly and circularly polarized patch antennas will be considered next.

2.6 Applications

a. Rectangular Patch

Rectangular patch antennas have been analyzed by a number of investigators [4, 5, 11]. Here we shall demonstrate the application of the GTLM to that patch.

The geometry of the patch is shown in Fig. 2.5. Suppose the patch is operated near the resonance of the TM_{01} mode. In that case, the maximum radiation takes place from the aperture at $y = 0$ and $y = b$ and the apertures at $x = 0$ and $x = a$ radiate very little amount of power.

According to the present model, the transmission line should be considered along the y-direction. The leakage of power from the walls of $x = 0$ and $x = a$ can be attributed to the complex propagation constant which is estimated in the following way.

The electric field component E_z inside the patch metallization can be expressed as

$$E_z = A(e^{jk_x x} + Be^{-jk_x x})(e^{jk_y y} + Ce^{-jk_y y}) \tag{51}$$

with $k_x^2 + k_y^2 = k_1^2$. The magnetic field components H_x and H_y are obtained from the Maxwell equation

$$\overline{H} = -\frac{1}{j\omega\mu}\nabla \times \overline{E} \tag{52}$$

The propagation constant k_x can be determined from the impedance boundary conditions at the transverse walls. Using that, we have

$$y_t = \left.\frac{H_y}{E_z}\right|_{\text{at } x = 0} = \left.\frac{-H_y}{E_z}\right|_{\text{at } x = a} \tag{53}$$

where y_t is the transverse wall admittance. Combining (51), (52) and (53), we have

$$y_t = -\frac{k_x}{\omega\mu}\left[\frac{1 - B}{1 + B}\right] = \frac{k_x}{\omega\mu}\left[\frac{e^{jk_x a} - B\,e^{-jk_x a}}{e^{ik_x a} + B\,e^{-jk_x a}}\right] \tag{54}$$

When y_t is known, we can solve for k_x from (54) using a numerical iteration technique. However, for a thin substrate, we can approximately obtain the expression for k_y in the following manner. When the thickness of the substrate is small, y_t is also very small and the value of B is approximately equal to unity. Equation (54) reduces to

$$y_t = \frac{jk_x}{\omega\mu}\tan(k_x a) \tag{55}$$

Again, it is assumed that the small radiation from the transverse walls yield a slight perturbation to k_x from the zero value. Then we have

$$k_x^2 = -j\omega\mu y_t/a$$

The propagation constant in the y-direction, k_y, is then

$$k_y = \left(k_1^2 - \frac{j\omega\mu}{a} y_t\right)^{1/2}$$

The imaginary part of y_t is very small compared to k_1^2 and therefore, k_y can be approximated as

$$k_y \simeq k_1 + \frac{j\,188\,g_t}{a\sqrt{\varepsilon_r}} \tag{56}$$

where g_t is the real part of y_t.

In order to obtain the equivalent circuit of the patch, we set $u = y$, $x_1(u) = e^{jk_y u}$ and $x_2(u) = e^{-jk_y u}$ in (27), (28) and (29). The input impedance seen by the coaxial feed is obtained as

$$Z_{in} = Zh/a \tag{57}$$

where Z is the impedance seen by the source current, I_s, in the equivalent circuit of Fig. 2.4. This current is related to the feed current, I_0, through equations (47) and for the TM_0 mode, the relation is given by

$$I_s = -I_0/a \tag{58}$$

In order to determine the input impedance Z, seen by I_s in Fig. 2.4, the expressions for the wall admittances y_1^s, y_2^s and y_{12}^m are to be known. These admittances can be obtained using the near field integration technique, coupled with the stationary expression. By using that procedure [12], the mutual admittance, y_{12}^m, is obtained as

$$y_{12}^m = \frac{jh \iint\limits_{x\,x'} f(x) f(x') \frac{e^{-jkr}}{r^3} \left[(1 + jkr)(2 - \frac{3d^2}{r^2}) + k^2 d^2\right] dx'dx}{2\pi\omega\mu \int\limits_x f^2(x)\,dx} \tag{59}$$

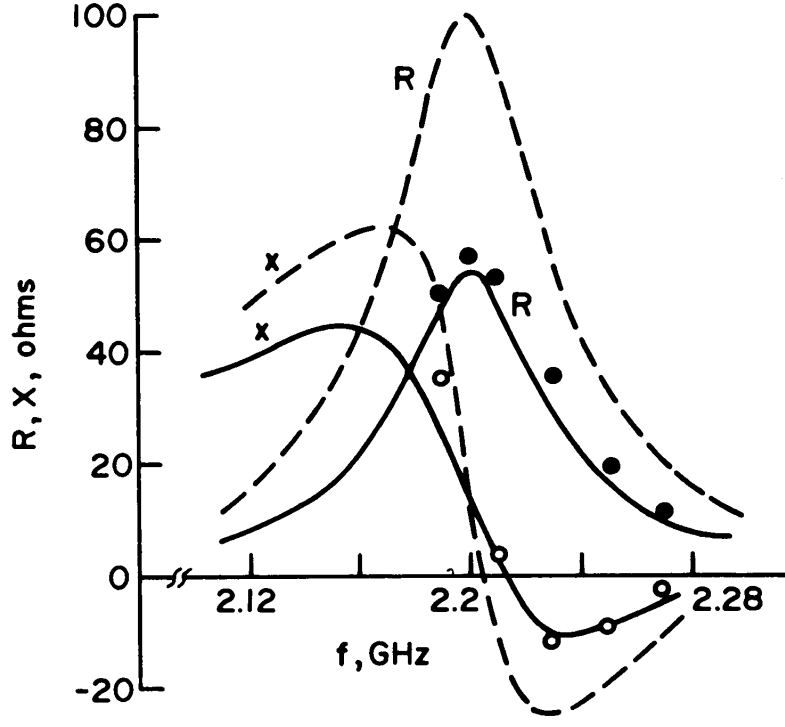

Figure 2.6 Input impedance of a rectangular patch antenna for the dominant mode (a = 6.858 cm, b = 4.14 cm, c = 1.016 cm, ε_r = 2.62, h = 0.159 cm) —— GTLM, ---- Transmission Line Model of Derneryd [5], • • • Experimental R, o o o Experimental X.

where $r^2 = (x-x')^2+d^2$ and $f(x)$ is the electric field distribution at the radiating wall separated by a distance d. For the walls at $x = 0$ and $x = a$ in Fig. 2.5, and for the TM_0 mode, $f(x) = 1$. The self conductances g_1^s and g_2^s can be obtained by setting $d = 0$ in (59) and retaining the real part. However, the self susceptances cannot be calculated using (59) as the apertures were assumed to be infinitely thin in deriving (59). The self susceptance can be estimated from the equivalent extension of the fringing fields. For the transverse conductance, g_t, used in (56), we set $f(x) = \cos(\pi x/b)$, $d = 0$ and integrate along the side wall.

The input impedance obtained from the GTLM was compared

with the measured data in Fig. 2.6. The dimension of the patch was: $a = 6.858$ cm, $b = 4.14$ cm, $c = 1.016$ cm, $\varepsilon_r = 2.62$ and $h = 0.159$ cm. In the theoretical calculation, a probe reactance of 14 ohms was used [1]. The diameter of the probe was 0.125 cm. Also shown in the figure are the computed values based on the earlier transmission line model [5]. From the figure, it is found that there is a closed agreement between the measured result and the result obtained from the GTLM. The discrepancy between the earlier transmission line model and the GTLM is due to the mutual coupling effect between the two radiating walls.

The GTLM can also be employed for a nearly square patch normally used to generate a circularly polarized radiated field. In such a case, two spatially orthogonal modes being excited, two different transmission lines (along x-direction and along y-direction) should be considered representing these two modes. The input impedance in this case will be the sum of input impedances due to both.

b. Circular Geometry

The separability criteria in (6) being satisfied for a circular geometry, the GTLM can be employed to determine the radiation characteristics of an annular ring patch antenna [13]. The earlier transmission line model [4, 5], on the other hand, is not applicable to analyze circular patches. The geometry of an annular ring is shown in Fig. 2.7. The scale factors (cylindrical coordinate system) are

$$h_1 = 1$$
$$h_2 = \rho = u$$

and

$$x_1(u) = J_n(k_1 u)$$
$$x_2(u) = Y_n(k_1 u)$$

where J_n and Y_n are respectively the Bessel and the Neumann functions of order n and k_1 is the wave number in the substrate medium. The v-dependence ($v = \phi$) of the field is

$$f_2(v) = \cos n\phi$$

[1] The probe reactance is calculated from the relation $x_p = \omega\mu_o h \ln(4/\gamma k_1 d)$, where $\gamma = 1.781$ and d is the diameter of the probe.

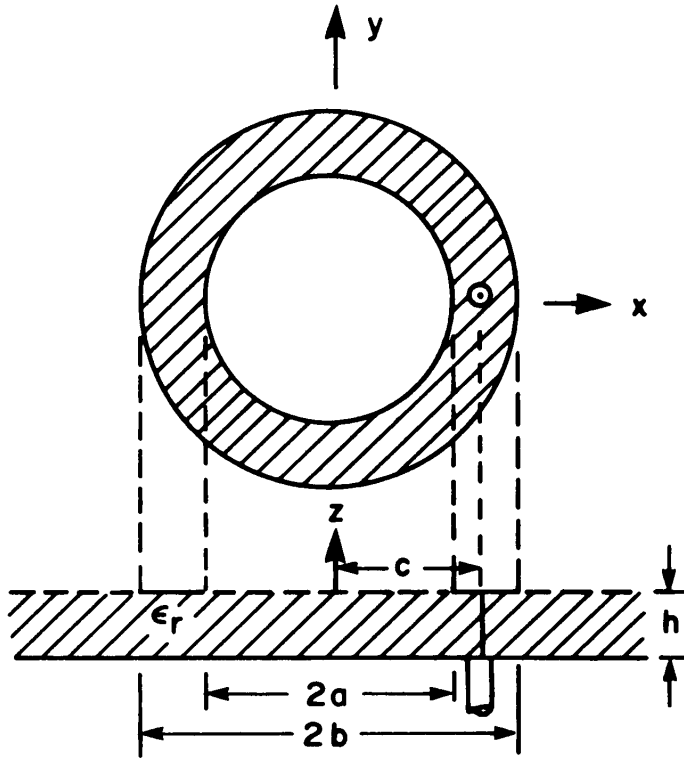

Figure 2.7 Annular ring patch antenna.

By using equations (27), (28) and (29), the lumped circuit elements in Fig. 2.4 are obtained. These are given by (in the region $b < \rho < c$)

$$g_1 = Y_{11} + Y_{12} = -\frac{j}{\omega\mu\Delta(b,c)}[k_1 b\Delta_1(b,c) + 2/\pi] \tag{60}$$

$$g_2 = -Y_{12} = -\frac{2j}{\pi\omega\mu\Delta(c,b)} \tag{61}$$

$$g_3 = Y_{22} + Y_{12} = \frac{j}{\omega\mu\Delta(c,b)}[k_1 c\Delta_1(c,b) + 2/\pi] \tag{62}$$

with

$$\Delta(b,c) = J_n(k_1 b)\,Y_n(k_1 c) - Y_n(k_1 b)\,J_n(k_1 c)$$

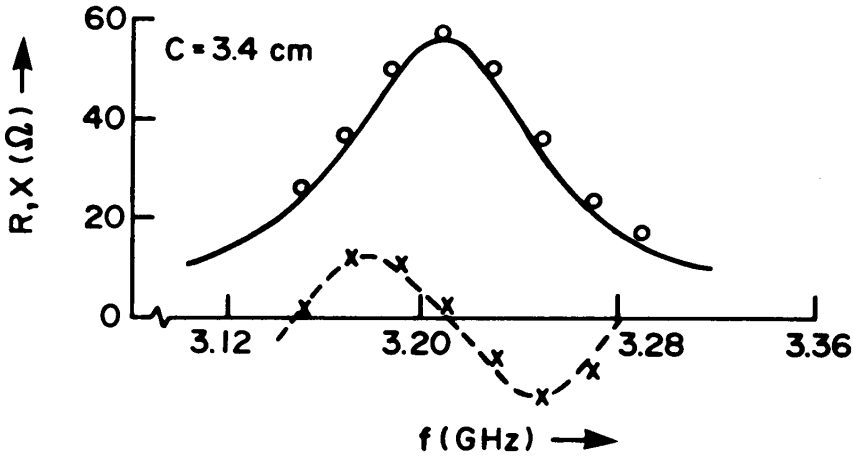

Figure 2.8 Input impedance of annular ring seen by a coaxial feed near the TM_{12} mode. ($a = 3$ cm, $b = 6$ cm, $c = 3.4$ cm, $\varepsilon_r = 2.2$) —— R, ---- X, o o o R (measured), × × × X (measured).

and

$$\Delta_1(b,c) = J_n'(k_1 b)\, Y_n(k_1 c) - Y_n'(k_1 b)\, J_n(k_1 c)$$

where the primes indicate derivatives with respect to the arguments. Expressions for the lumped elements in the region $a < \rho < c$ can be obtained by replacing b by c and c by a in (60), (61) and (62). The mutual wall admittance y_{12}^m is derived as [12]

$$y_{12}^m = \frac{jabh}{2\pi\omega\mu} \int_0^{2\pi} \cos\alpha \frac{e^{-jkr}}{r^3} \left[2(1+jkr)\cos\alpha + \frac{(b\cos\alpha - a)(b - a\cos\alpha)}{r^2} (k^2 r^2 - 3jkr - 3) \right] d\alpha \tag{63}$$

with

$$r^2 = a^2 + b^2 - 2ab\cos\alpha$$

The self conductance can be obtained from (63) by setting $b = a$ and retaining the real part. The self susceptance is obtained from the equivalent extension formula [1].

The equivalent network in Fig. 2.4 was simplified in [13] using the delta to star and star to delta transformation and the input impedance was obtained. In Figure 2.8, the computed results for the input impedance are plotted against frequency. Also given in the figure are the measured impedances. The agreement between the theoretical and experiment results is good. In calculating the total input reactance, the reactances for the neighboring modes (TM_{02} and TM_{51}) are also added to that of the TM_{12} mode. The input resistances, however, were estimated from the TM_{12} mode alone [13].

The GTLM was employed to determine the radiation characteristics of an annular ring patch antenna with an ear at the outer periphery. If the ear is placed at an angle 45° with the feed location, a circularly polarized radiated field in the broad side direction can be achieved. Due to the asymmetry of the structure caused by the ear, the two modes (even and odd) degenerate and a 90° phase difference between the amplitudes of the aperture fields is obtained which gives rise to a circularly polarized wave. In order to analyze this structure, two equivalent circuits for two modes (even and odd) are to be considered [14]. The input impedance seen by the feed is equal to the sum of the individual impedances. The effect of the extended ear comes through a reactance loaded at one end in the equivalent circuit of the even mode. For the odd mode, the effect of the ear is negligibly small since the odd mode field has a null at the location of the ear.

The methodology was applied successfully and the computed input impedances were compared with the experimental data. Figure 2.9 shows the comparison. A feed reactance of 23.5 ohms (inductive) has been subtracted from the experimental input impedance. Two peaks of the resistance curve are due to the presence of the two modes (TM_{12} even and odd). The radiation pattern of the antenna was also measured. The measured result [14] is shown in Fig. 2.10. The measured pattern shows a very good circularly polarized wave in the broad side direction. Away from the broad side, the axial ratio of the circular polarization deteriorates which is basically due to the difference in the E and the H-plane patterns of the ring.

Annular and circular sector microstrip patch antennas were also analyzed [15] using the GTLM. The leakage of power from the side walls was accounted from the complex order of the Bessel and the Neumann functions [15]. Experimental results for the input impedance and radiation pattern show a good agreement with the theory. The

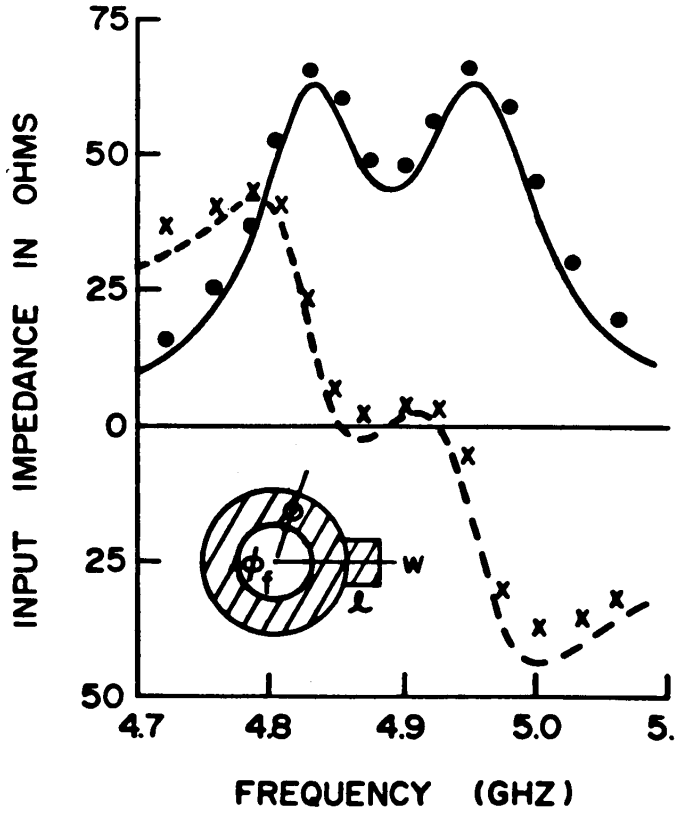

Figure 2.9 Theoretical and experimental input impedance of an annular ring antenna with an ear at the outer periphery (for the TM_{12} mode of operation). $a = 1$ cm, $b = 3$ cm, $c = 1.5$ cm, $\phi_f = 45°$, $\varepsilon_r = 2.52$, $h = 0.159$ cm, w = 1.0 cm, $\ell = 0.4$ cm. —— R, ---- X (Theory), • • • R, × × × X (Measured).

semicircular annular sector exhibits a larger bandwidth as compared to a circular sector and circular patch antenna

c. Elliptical Ring

The separability criteria is satisfied for elliptical geometry and therefore the GTLM is applicable for this kind of patch shapes. This

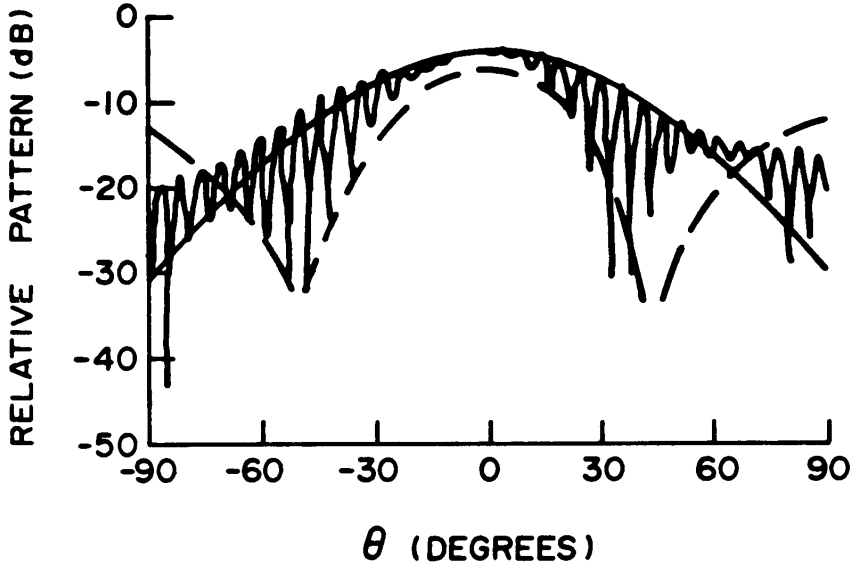

Figure 2.10 Measured radiation pattern (using rotating linear antenna for circular polarization measurement) of the annular ring described in Fig. 2.9. $f = 4.9$ GHz.

model was used to obtain the radiation characteristics of a confocal elliptical ring microstrip antenna [16]. This patch shape supports two types of modes (even and odd) which are symmetrical about the minor and the major axes, respectively. Each mode has its equivalent circuit shown in Fig. 2.4. For the even mode, the expressions for $x_1(u)$ and $x_2(u)$ were

$$x_1(u) = R_{em}^{(1)}(c_0 k_1, \xi) \tag{64}$$

$$x_2(u) = R_{em}^{(2)}(c_0 k_1, \xi) \tag{65}$$

where k_1 is the wave number in the free space, c_0 is the distance of focii from the center of the ellipse, and $\xi = \cosh u$. R is the radial Mathieu's function and the subscript e stands for the even function.

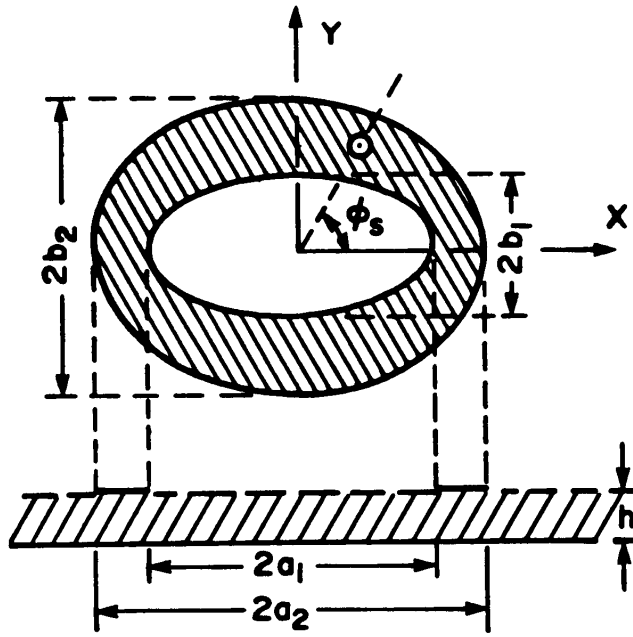

Figure 2.11 Geometry of a confocal elliptical ring antenna.

The superscripts (1) and (2) represent the first and the second kinds, respectively. The circumferential variation of the electric field for the even mode is

$$f_2(v) = S_{em}(c_0 k_1, \cos v) \tag{66}$$

Expressions for the Mathieu's functions are given in reference [17] in the infinite series forms. For the odd modes, the radial variation of the electric field consists of odd Mathieu's functions [16].

From the theoretical results, it was found that if the ratio between the minor and the major axes of the outer ellipse is in the range of 0.98 to 0.99 and for the inner ellipse the ratio lies between 0.92 to 0.96, a good circularly polarized wave can be achieved. The feed location for a circularly polarized wave, however, should be at an angle of about 45° from the major axis (Fig. 2.11). An experimental pattern of an elliptical ring is shown in Fig. 2.12. The axial ratio in the broad side direction is less than 1 dB. The directive gain of the radiation is about

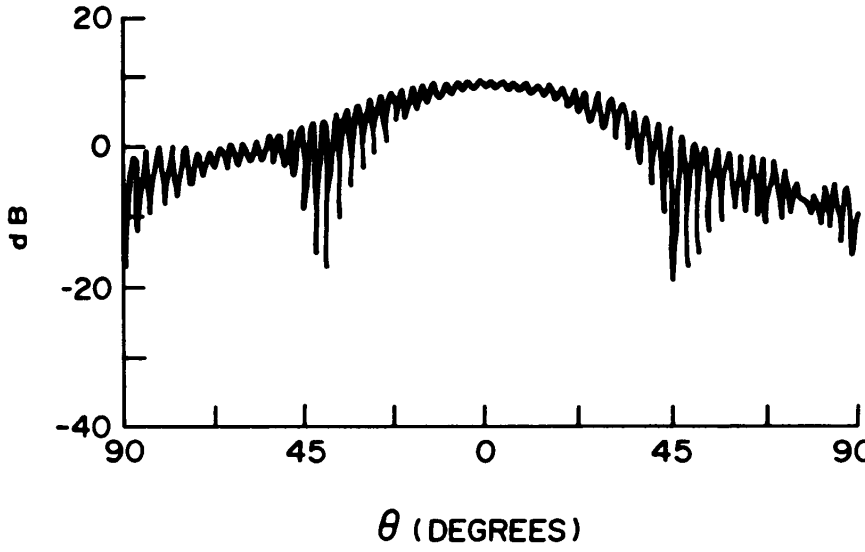

Figure 2.12 Measured radiation pattern (with rotating linear antenna as the receiver) of an elliptical patch antenna. $a_1 = 1.45$ cm, $b_1 = 1.34$ cm, $a_2 = 4.0$ cm, $b_2 = 3.96$ cm, a_s (the major axis of the fictitious ellipse on which the feed is located) $= 2.0$ cm, $\phi_s = 45°$, $\varepsilon_r = 2.55$, $h = 0.159$ cm, $f = 3.84$ GHz.

10 dB, which is 3 dB larger compared to an elliptical patch [2] (which also gives a circularly polarized wave) [18]. The axial ratio band width of the elliptical ring is larger than an elliptical patch (Fig. 2.13).

A very important difference between the elliptical patch and elliptical ring antenna was noted. In order to obtain a left handed circularly polarized wave from an elliptical patch, the feed location should be at an angle $+45°$ with the major axis [18]. The above angle is $-45°$ for an elliptical ring [16]. The reason behind this difference is explained from the resonant frequency of the even and odd modes. In the case of

[2] This is due to the fact that the elliptical ring has two radiating apertures whereas an elliptical patch has only one radiating edge. Moreover, the size of an elliptical ring is larger than that of an elliptical patch for the same resonant frequency.

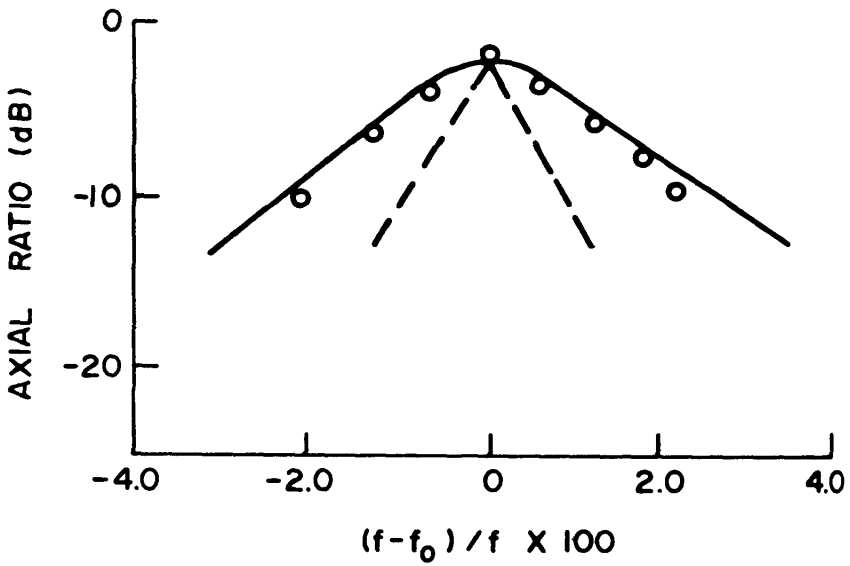

Figure 2.13 Variation of axial ratio with frequency for elliptical patch and elliptical ring antennas. ---- Elliptical patch, —— Elliptical Ring (Theory), o o o (measured, elliptical ring).

an elliptical patch, the even mode has a lower resonant frequency than that of the odd mode, so that at the center frequency (mid frequency between two resonances) the odd mode leads in phase. On the other hand, for the elliptical ring, the odd mode resonates before the even mode and at the center frequency the even mode leads in phase. Therefore, if the relative location of the feed is $+45°$ with the major axis, the two structure yield two opposite types of polarization. In addition to the above difference, the elliptical ring is superior to an elliptical patch in terms of gain and band width [16].

2.7 Conclusions

In this chapter, we have discussed the mathematical foundation of the GTLM. It is also demonstrated with example, how this model can

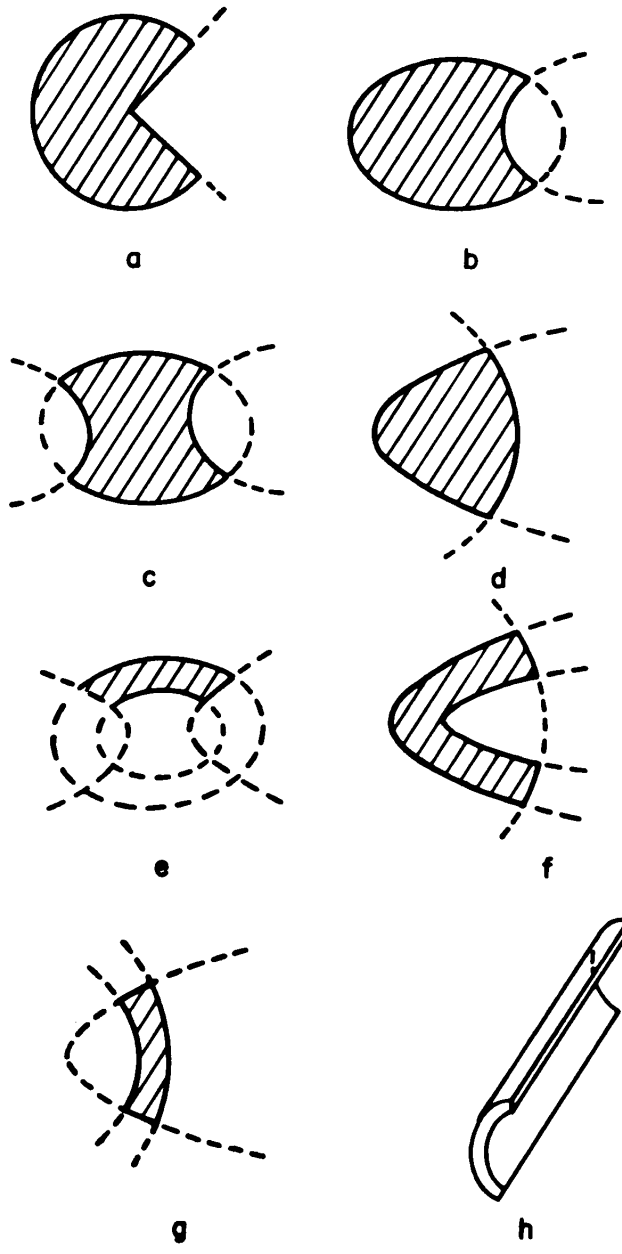

Figure 2.14 Some microstrip patch configurations with separable geometry where the GTLM can be applied.

be employed to determine the impedance and radiation characteristics of various patch shapes. A few more patch geometries for which the GTLM is applicable are shown in Fig. 2.14. These are: circular and elliptical disks with one or more sectors removed, parabolic shaped disks, elliptic sector, parabolic sector, etc. The model can be extended to analyze patches on a cylinder as on a sphere, which satisfy separability criteria. In addition to these geometries, the GTLM is applicable to the following cases:

i) Patch with slots and shorting pins: For some special applications, such as obtaining a circular polarization from a linearly polarized patch antenna, a slot is cut on the patch metallization. The cavity model is not suitable for analyzing such kind of slotted patches. The GTLM can be employed to analyze these structures. The slot is replaced by an equivalent magnetic current source. The modal current and modal voltage will be discontinuous at the location of the slot, due to the presence of the magnetic current. From the discontinuity, the equivalent Π-network of the slot can be determined using the procedure given in the literature [19]. The equivalent Π-network of the slot together with the equivalent circuit of the patch yield the equivalent circuit of the slotted patch antenna. Equivalent circuit of a patch with a shorting pin can be obtained in a similar manner.

ii) Non-separable patches: The application of the GTLM can be extended to these patch shapes which can be approximated by the shapes with separable geometries. As for example, an isosceles triangular patch with an angle less than 60° can be approximated as a circular sector which has a separable geometry. In order to have an accurate result, the radius of the sector should be chosen in such a way that the area of the triangle becomes equal to that of the circular sector. Except for some selective angles, the cavity model cannot be used to analyze triangular patches [1].

To sum up, the GTLM described here is capable of analyzing most of the microstrip patches with a good accuracy. Although it is a piecemeal approach (mutual admittance and self admittances are determined separately and included in the equivalent circuit) compared to the integrated approach of moment method, the GTLM provides a clear picture of mechanism of radiation and the influence of various parameters on the antenna characteristics.

Appendix A: Wronskian of equation (8)

Let $x_1(u)$ and $x_2(u)$ be two independent solutions of (8). Then each solution will satisfy the differential equations and therefore,

$$\frac{\partial^2 x_1}{\partial u^2} + \frac{1}{g}\frac{\partial g}{\partial u}\frac{\partial x_1}{\partial u} + \frac{(k_1^2 m_1 - \alpha^2)}{g^2} x_1 = 0 \qquad \text{(A.1)}$$

and

$$\frac{\partial^2 x_2}{\partial u^2} + \frac{1}{g}\frac{\partial g}{\partial u}\frac{\partial x_2}{\partial u} + \frac{(k_1^2 m_1 - \alpha^2)}{g^2} x_2 = 0 \qquad \text{(A.2)}$$

Multiplying (A.1) by x_2 and (A.2) by x_1 and subtracting we can derive

$$\frac{dW_1}{du} + \alpha_1 W_1 = 0 \qquad \text{(A.3)}$$

where W_1 is the Wronskian of (8), defined as

$$W_1 = x_1 \frac{\partial x_2}{\partial u} - x_2 \frac{\partial x_1}{\partial u}$$

and

$$\alpha_1 = \frac{1}{g}\frac{\partial g}{\partial u}$$

The solution to (A.3) is

$$W_1(u) = A e^{-\int \alpha_1 \, du} = \frac{A}{g(u)} \qquad \text{(A.4)}$$

where A is a constant. Substituting the expression of $g(u)$ from (6a), we have

$$W_1(u) = C \frac{h_1}{h_2} f(v)$$

Appendix B: Solutions of equation (9) are orthogonal

Let $f_2^{(1)}(v)$ and $f_2^{(2)}(v)$ are two solutions of (9) with eigenvalues α_1 and α_2, respectively. These solutions either follow the magnetic wall boundary conditions at $v = v_1$, and $v = v_2$ (Fig. 2.1(b)) or they are periodic functions of v (in the case of Fig. 2.1(a)). The orthogonality can be proved if any one of the above two conditions are satisfied.

Substituting $f_2(v) = f_2^{(1)}(v)$ and $\alpha = \alpha_1$ in (9) we obtain

$$\frac{\partial^2 f_2^{(1)}}{\partial v^2} - \frac{1}{f}\frac{\partial f}{\partial v}\frac{\partial f_2^{(1)}}{\partial v} + (k_1^2 m_2 + \alpha_1^2) f^2 f_2^{(1)} = 0 \qquad \text{(B.1)}$$

Similarly, substituting $f_2(v) = f_2^{(2)}(v)$ and $\alpha = \alpha_2$, we have

$$\frac{\partial^2 f_2^{(2)}}{\partial v^2} - \frac{1}{f}\frac{\partial f}{\partial v}\frac{\partial f_2^{(2)}}{\partial v} + (k_1^2 m_2 + \alpha_1^2) f^2 f_2^{(2)} = 0 \qquad \text{(B.2)}$$

Multiplying (B.1) by $f_2^{(2)}$ and (B.2) by $f_1^{(2)}$ and subtracting them one gets

$$\frac{\partial}{\partial v}\left(\frac{F}{f}\right) + (\alpha_2^2 - \alpha_1^2) f\, f_2^{(1)} f_2^{(2)} = 0 \qquad \text{(B.3)}$$

where

$$F(v) = f_2^{(1)}\frac{\partial f_2^{(2)}}{\partial v} - f_2^{(2)}\frac{\partial f_2^{(1)}}{\partial v} \qquad \text{(B.4)}$$

Integrating (B.3) with respect to v (from v_1 to v_2) we have

$$(\alpha_2^2 - \alpha_1^2)\int_{v_1}^{v_2} f f_2^{(1)}(v) f_2^{(2)}(v)\, dv = -\frac{F(v_2)}{f(v_2)} + \frac{F(v_1)}{f(v_1)} \qquad \text{(B.5)}$$

If the contour is closed (Fig. 2.1(a)), v_2 and v_1 are equal and the right of (B.5) is zero. This yields

$$\int_{v_1}^{v_2} f\, f_2^{(1)}(v)\, f_2^{(2)}(v)\, dv = 0$$

indicating that $f_2^{(1)}$ and $f_2^{(2)}$ are orthogonal.

If the contours are not closed as in Fig. 2.1(b), the magnetic wall boundary conditions at $v = v_1$ and $v = v_2$ is assumed. In such a situation,

$$\left.\frac{\partial f_2^{(1)}}{\partial v}\right|_{v=v_1} = \left.\frac{\partial f_2^{(1)}}{\partial v}\right|_{v=v_2} = \left.\frac{\partial f_2^{(2)}}{\partial v}\right|_{v=v_1} = \left.\frac{\partial f_2^{(2)}}{\partial v}\right|_{v=v_2} = 0$$

and therefore $F(v_2) = F(v_1) = 0$, which also proves the eigenfunctions $f_2^{(1)}$ and $f_2^{(2)}$ are orthogonal.

Appendix C: Expression for y_{12}^m in (49) is stationary

Let $f_2(v)$ be the exact field distribution on the apertures at $u = u_1$ and $u = u_2$. Then by definition,

$$y_{12}^m = \frac{-h_2\, H_{vm}(u_1, u_2)}{E_z(u_2)} = \frac{h_2\, H_{vm}(u_2, u_1)}{E_z(u_1)} \tag{C.1}$$

where $f_2(v)\, H_{vm}(u_1, u_2)$ is the v-component of the magnetic field on the aperture at $u = u_1$ produced by the aperture at $u = u_2$. $E_z(u_2) f_2(v)$ is the electric field at $u = u_2$.

The expression for $H_{vm}(u_1, u_2)$ can be obtained using the Green function technique. Using that, one can have

$$f_2(v)\, H_{vm}(u_1, u_2) = hE_z(u_2) \int_{v_1}^{v_2} f_2(v')(\hat{v}' \cdot \overline{\overline{G}} \cdot \hat{v})\, h_2(v')\, dv' \tag{C.2}$$

where $\overline{\overline{G}}$ is the dyadic Green's function which relates the magnetic current to the magnetic field. $\hat{v}$ and $\hat{v}'$ are the unit vectors along the v-direction on the apertures at $u = u_1$ and $u = u_2$, respectively. Combining (C.1) and (C.2), we have

$$y_{12}^m = \frac{-h\, h_2(v) \displaystyle\int_{v_1}^{v_2} f_2(v')(\hat{v}' \cdot \overline{\overline{G}} \cdot \hat{v}) h_2(v')\, dv'}{f_2(v)} \tag{C.3}$$

Now let us assume that the trial aperture field distribution differs slightly from the actual aperture field distribution. Let the trial field distribution be

$$f_2^{(t)}(v) = f_2(v) + \Delta f_2(v)$$

If we determine y_{12}^m using (3.3) and substitute $f_2(v) = f_2^{(t)}(v)$, we will end up with some error in y_{12}^m. The error in y_{12}^m (first order) is given by the following equation:

$$f_2(v)\Delta y_{12}^m + \Delta f_2(v) y_{12}^m = -h\, h_2(v) \int_{v_1}^{v_2} \Delta f_2(v')(\hat{v}')(\hat{v}' \cdot \overline{\overline{G}} \cdot \hat{v}) h_2(v') dv'$$

or

$$\Delta y_{12}^m = -\frac{\Delta f_2(v)}{f_2(v)} y_{12}^m - \frac{h\, h_2(v)}{f_2(v)} \int_{v_1}^{v_2} \Delta f_2(v')(\hat{v}' \cdot \overline{\overline{G}} \cdot \hat{v}) h_2(v') dv' \tag{C.4}$$

Note that the error in $y_{12}^m(\Delta y_{12}^m)$ is of the same order of Δf_2. This indicates that (C.1) does not yield a stationary expression for y_{12}^m.

We now examine the error in y_{12}^m if it is calculated from (49). The mutual reaction if given by

$$\begin{aligned}\langle u_1, u_2\rangle &= -h \int_v H_{vm}(u_1, u_2)\, f_2(v)\, E_z(u_1)\, f_2(v) h_2(v)\, dv \\ &= -h^2 E_z(u_1)\, E_z(u_2) \int_v \int_{v'} f_2(v)\, f_2(v')(\hat{v}' \cdot \overline{\overline{G}} \cdot \hat{v}) \\ &\qquad h_2(v) h_2(v')\, dv' dv\end{aligned}$$

Therefore, y_{12}^m becomes

$$y_{12}^m = \frac{-h \int_v \int_{v'} f_2(v)\, f_2(v')(\hat{v}' \cdot \overline{\overline{G}} \cdot \hat{v}) h_2(v)\, h_2(v')\, dv' dv}{\int_v f_2^2(v)\, dv} \tag{C.5}$$

If we replace $f_2(v)$ by $f_2(v) + \Delta f_2(v)$ in (C.5), we can have the following equation for the first order error in y_{12}^m.

$$\begin{aligned}&2y_{12}^m \int_v f_2(v) \Delta f_2(v)\, dv + \Delta y_{12}^m \int_v f_2^2(v) dv \\ &\quad = -h \int_v \int_{v'} \Delta f_2(v) f_2(v')(\hat{v}' \cdot \overline{\overline{G}} \cdot \hat{v})\, h_2(v)\, h_2(v')\, dv'\, dv \\ &\qquad - h \int_v \int_{v'} f_2(v) \Delta f_2(v')(\hat{v}' \cdot \overline{\overline{G}} \cdot \hat{v})\, h_2(v)\, h_2(v')\, dv' dv\end{aligned}$$

The dyadic Green's function being symmetric with respect to v and v', the two integrals on the right of the foregoing equation are equal. Therefore,

$$\begin{aligned}\Delta y_{12}^m \int_v f_2^2(v)\, dv &= -2y_{12}^m \int_v f_2(v) \Delta f_2(v)\, dv \\ &\qquad - 2h \int_v \int_{v'} f_2(v') \Delta f_2(v)(\hat{v}' \cdot \overline{\overline{G}} \cdot \hat{v})\, h_2(v)\, h_2(v')\, dv' dv\end{aligned}$$

Rearranging the above equation, one has

$$\Delta y_{12}^m \int_v f_2^2(v)dv = -2 \int_v \Delta f_2(v) \left[f_2(v) y_{12}^m + \left\{ h \int_{v'} f_2(v') \right. \right.$$
$$\left. \left. (\hat{v}' \cdot \overline{\overline{G}} \cdot \hat{v}) h_2(v') dv' \right\} h_2(v) \right] dv \qquad \text{(C.6)}$$

Now if we combine (C.3) and (C.6) we obtain

$$\Delta y_{12}^m = 0$$

which indicates that the first order error in y_{12}^m is zero. This proves the stationary character for the expression of y_{12}^m in equation (49). In a similar way expression in (50) can also be proved to be stationary.

References

[1] Bahl, I. J., and P. Bhartia, *Microstrip Antenna*, Artech House, 1980.

[2] James, J. R., P. S. Hall, and C. Wood, *Microstrip Antenna, Theory and Design*, Peter Peregrinus, 1981.

[3] Carver, K. R., and J. W. Mink, "Microstrip antenna technology (invited)," *IEEE Trans.*, Vol. **AP-29**, 2–24, 1981.

[4] Munson, R. E., "Conformal microstrip antennas and microstrip phased arrays," *IEEE Trans.*, Vol. **AP-22**, 74–78, 1974.

[5] Derneryd, A. G., "Linearly polarized microstrip antennas," *IEEE Trans.*, Vol. **AP-24**, 846–851, 1976.

[6] Derneryd, A. G., "A Theoretical investigation of the rectangular microstrip antenna element," *IEEE Trans.*, Vol. **AP-26**, 532–535, 1978.

[7] Bhattacharyya, A. K., and R. Garg, "Spectral domain analysis of wall admittances for circular and annular microstrip patches and the effect of surface waves," *IEEE Trans.*, Vol. **AP-33**, 1067–1073, 1985.

[8] Bhattacharyya, A. K., and R. Garg, "Generalized Transmission Line Model for Microstrip Patches," *Proceedings of Ins. of Elect. Eng.*, Vol. **132**, Pt. H, No. 2, 93–98, 1985.

[9] Morse, P. M., and H. Feshback, *Methods of Theoretical Physics*, McGraw-Hill, New York, 1953.

[10] Kong, J. A., *Electromagnetic Wave Theory*, Wiley-Interscience, New York, 1986.

[11] Lo, Y. T., D. Solomon and W. F. Richards, "Theory and experiments on microstrip antennas," *IEEE Trans.*, Vol. **AP-27**, 137–145, 1979.

[12] Bhattacharyya, A. K. and R. Garg, "Self and mutual admittances between two concentric, coplaner, circular radiating current sources," *Proc. Inst. of Elec. Eng.*, Pt. H, Vol. **131**, 217–219, 1984.

[13] Bhattacharyya, A. K., and R. Garg, "Input impedance of annular ring microstrip antenna using circuit theory approach," *IEEE Trans.*, Vol. **AP-33**, 369–374, 1985.

[14] Bhattacharyya, A. K., and L. Shafai, "A wider band microstrip antenna for circular polarization," *IEEE Trans.*, Vol. **AP-36**, 157–163, 1988.

[15] Bhattacharyya, A. K., and R. Garg, "Analysis of annular sector and circular sector microstrip patch antennas," *Electromagnetics*, Vol. **6**, No. 3, 229–242, 1986.

[16] Bhattacharyya, A. K., and L. Shafai, "Theoretical and experimental investigation of the Euiptical Annular Ring Antenna," *IEEE Trans.*, Vol. **AP-36**, 1526–1530, 1988.

[17] Abramowitz, M., and I. A. Stegun, *Handbook of Mathematical Functions*, Dover, New York, 1968.

[18] Shen, L. C., "The Elliptical microstrip antenna for circular polarization," *IEEE Trans.*, Vol. **AP-29**, 90–94, 1981.

[19] Silver, S., *Microwave Antenna Theory and Design*, (Edited book), Chapter 9, 1949.

[20] Pues, H., and A. Van de Capelle, "Accurate transmission-line model for the Rectangular Microstrip Antenna," *Proc. Ins. Elect. Eng.*, Pt. H, 334–340, Dec. 1984.